L'Université d'Aix-Marseille

CENTRE DE PHYSIQUE DES PARTICULES DE MARSEILLE

Master Thesis

The study of the data and simulation agreement for the lepton flavor violating $\tau \to K^0_s l$ analysis at Belle II.

Author :
Esraa Khidr

Supervisor :
Klemens Lautenbach

acknowledgment

First and foremost, my endless grateful for my supervisor, Klemens Lautenbach whose guidance, patience, support was a constant presence throughout the internship of this project. Thank you so much for your comments, discussions, and teaching that was invaluable to this analysis and thesis. Much obliged for giving me the self confidence and your happy face since you welcomed me. This project would not have been what it is without your greater suggestions, the fantastic advice and the greater efforts. My deep thanks for having my back, you have all my respect and appreciation.
Also, I would like to send my biggest thanks to the Belle II group at CPPM for their attention and comments during the meetings, you were the best team I worked with and I wish you success in all future. Thanks also go to the CPPM stuff for the hospitality and creating a very great work atmosphere, many thanks to all of you.
Professor Serge LAZZARINI, words of thanks are not enough for you, I will not forget your favor for the rest of my life. My deepest thanks for accepted me and your great help to all the student and make them in their home. Many thanks for keep us calm and your effort to make life easier, the dream has become true because of you, Prof, Serge.
My biggest grateful to my family(Dad, Mom, Grand Mom, brothers and my sister), thank you so much of believing in me and your moral support. Whenever, I remember my difficult days, I remember your fatigue for me, your pray and your love, many thanks.
My Dady, the role model and my first support during all my journey, I confess your great effort and I hope I achieve more progress to make you proud and happy.
Finally, I would like to thank my best friend Noha, of being emerges in times of adversity and trying to motivated me during my studies.

Contents

1 Introduction

Thanks to the Standard Model of being an influential theory that contributes to the discovery of elementary particle physics and the nature of their interactions with matter. SM helps scientists to discover the secrets of the universe and it succeeded in discovering many particles through experimental observations and discoveries validating many of its features. Among them, the discovery of gluons (DESY, 1979), the τ (SLAC, 1976) and ν_τ (FNAL, 2000) leptons, and the $W^\pm$ and Z gauge bosons (CERN 1983). The most recently unprecedented discovery is the Higgs Boson (CERN, 2012), responsible for the origin of mass in fundamental particles.
Despite its great success, the Standard Model is not sufficient to answer some phenomena observed recently. For example, the discovery of neutrino oscillation results in a lepton flavor violation which is forbidden in the SM. Physicists are studying, and probing extensions of the SM such as Super-Symmetry, CP-violation, and LeptoQuark model, to predict the branching ratios of lepton flavor violation decays which are expected to be larger and detectable with the current experiments.
Belle II experiment is aiming to search for a new physics in rare and forbidden decays through out collecting data set of high luminosity achieved with the particle accelerator SuperKEKB by collisions of electrons and positrons of different energies at the $\Upsilon(4S)$ resonance. The Belle II detector is supported by sub-detectors located around the interaction point of SuperKEKB. Due to the clean environment and high $\tau\bar{\tau}$ cross section, make the study of LFV in τ decays is perfect.
In this analysis, we focus on $\tau^\pm \to l^\pm K_s^0$ decay mode. To allow for a precise measurement of the branching fraction upper limit with systematic errors as small as possible, a detailed understanding of the data and simulation comparison is crucial, which we study in this report. The agreement between data and MC is performed in this analysis through the study of the trigger lines and the reconstruction process with some additional selections in order to reduce the background events.

2 Belle II experiment

Belle Experiment is located in Tsukuba (Japan) at the KEK laboratory, it was running from 1999 to 2010 for discovering CP violation in the B mesons After that time, an upgrade was planned and new components developed and employed for the successor experiment. Belle II experiment is considered the next-generation super B-factory, for searching for new physics in the flavor and CP violation sector, and observation of forbidden decays. This section will discuss the Belle II upgrades and their its sub-detectors, as well as the upgrades rolled out on the collider SuperKEKB.

2.1 SuperKEKB Collider

SuperKEKB is an asymmetric electron positron collider machine with a circumference of 3km, operating mainly at a center of mass energy of the $\Upsilon(4S)$ resonance. The goal is to reach a design luminosity of $8 \times 10^{35} cm^{-2} s^{-1}$, leading to an integrated data set of 50 ab^{-1} over the experiment lifetime. This section will discuss how to accomplish the higher luminosity,

- First, **Nano-beam scheme**, is aiming to resize the beam from 1 $\mu m \rightarrow$ 50 nm (20 times smaller than in Belle). This is achieved by squeezing the transversal dimension of electron and positron beams at the interaction point, in other words, reducing the cross-section area of $e^- e^+$ collision. The luminosity of accelerated beams is,

$$\mathcal{L} = \frac{\gamma_\pm}{2er_e} \frac{R_L}{R_{\zeta_y}} \frac{I_\pm \zeta_{y,\pm}}{\beta^*_{y,\pm}} \tag{1}$$

  Where $\pm$ sign refers to the electron(-) and positron(+),$\gamma_\pm$ is the Lorentz factor, r_e the electron radius, e is the elementary electric charge, $\frac{R_L}{R_{\zeta_y}} \approx 1$ refers to the reduction factor that comes from the beam-beam effect, which yields from the electromagnetic interaction between two charged beams. The accelerated charged particles produce a field, exerting a force on the beam itself and the opposite bunch generated after the collision, $I_\pm$ is the beam current, $\zeta_{y,\pm}$ is the vertical beam-beam parameter, $\beta^*_{y,\pm}$ is the vertical beta function or the "envelope function", , which is related to the vertical beam size σ_y thought this relation $\sigma_y = \sqrt{\epsilon \beta^*}$

  From equation1, one notice that β function is inversely proportional to the luminosity and that requires a small beam size to achieve high luminosity which is the idea behind nano-beam scheme. In this scheme 1, the crossing angle between two beams is $\phi = \frac{\sigma_x}{d}$

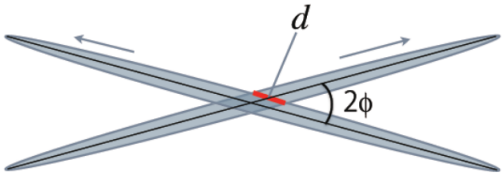

Figure 1: Nano-beam Scheme

  where σ_x is the horizontal beam (beam width), d is cross section area. In SuperKEKB, ϕ= 2.378°(=41.5 mrad), and σ_x = 7.75 μm, thus yields a d= 200 μm which leading to the vertical beta function is 20 times smaller.

- Second, **The energy of the electron and positron beam**: There are two accelerating rings, one for the electron beam, High Energy Ring HER and the positron beam, Low Energy Ring LER. The HER runs at 7 GeV and the LER at 4 GeV, leading to a 10.58 GeV center of mass (CM) energy. Due to the asymmetric energy of the rings, a Lorentz Boost of the laboratory frame with respect to the CM frame by a factor of $\beta\gamma$=0.28 is achieved.
  To illustrate this point, let's introduce how $\beta\gamma$ can be calculated mathematically:

– Center of Mass reference frame: consider two particles, a and b, with masses m_a and m_b are colliding together, to produce other particles. The net four-momenta are P_a = (E_a, $\vec{p_a}$) and P_b = (E_b, $\vec{p_b}$) and we define the total energy in the CM as ,

$$s = (P_a + P_b)^2 = (E_a^* + E_b^*)^2 - (p_a^* + p_b^*)^2 = (E_a^* + E_b^*)^2 \tag{2}$$

with $(p_a^* + p_b^*)^2$= 0, and from the conservation of energy, we have M= $(E_a^* + E_b^*)^2$ = $\sqrt{s}$.

– CM energy in the lab frame: the target is fixed and we consider, a is the beam particle and b is the target. In this case, $p_b = 0$, $E_b = m_b$. Then, P_a = (E_a, $\vec{p_a}$) and nd P_b = (m_b, 0), then the total energy is calculated as,

$$s = (P_a + P_b)^2 = m_a^2 + m_b^2 + 2m_b E_a \tag{3}$$

Now, since there is asymmetry in the beam energies, the question will be how fast is CM frame seen with respect to Lab frame? A combination between systems can be performed by the Lorentz transformation as,

$$\begin{pmatrix} E \\ p^* \end{pmatrix} = \begin{pmatrix} \gamma & \beta\gamma \\ \beta\gamma & \gamma \end{pmatrix} \begin{pmatrix} \sqrt{s} \\ 0 \end{pmatrix} \tag{4}$$

with E = E_a+m_b, and $p^* = \sqrt{E^2 - m^2}$, since electron and positron energies are very high, we can write $p^* = E = E_{e^-} - E_{e^+}$.
Equivalently,

$$\begin{pmatrix} E_a{+}m_b \\ E_{e^-} - E_{e^+} \end{pmatrix} = \begin{pmatrix} \gamma & \beta\gamma \\ \beta\gamma & \gamma \end{pmatrix} \begin{pmatrix} \sqrt{s} \\ 0 \end{pmatrix} \tag{5}$$

Written as a linear equation, $\beta\gamma = \frac{E_{e^-} - E_{e^+}}{\sqrt{s}}$, $E_a{+}m_b = \gamma\sqrt{s}$. So we have,

$$\beta = \frac{E_{e^-} - E_{e^+}}{E_a + m_b} \tag{6}$$

$$\gamma = \frac{E_a + m_b}{\sqrt{s}} \tag{7}$$

$$\beta\gamma = \frac{E_{e^-} - E_{e^+}}{\sqrt{s}} = \frac{7GeV - 4GeV}{10.58GeV} \approx 0.28 \tag{8}$$

Physically, this factor is causing the separation between B mesons at the decay vertices. Because the momentum of B mesons in CM is lower than in the Lab frame, their products will be boosted along the z direction. since one of the B-mesons lives longer than the other (decays later) it also decays further away from the common vertex of the beams. BUT the $\beta\gamma$ factor is less than in Belle and this is why Belle 2 needs a better vertex detector.

3 Belle II Detector

The Belle detector must be constructed in line with the high luminosity produced by the SuperKEKB to perform very precise measurements. Belle II detector has a length of 7.5 m and a diameter of almost 7 m, and it consists of sub-detectors that are constructed around the interaction point with cylindrical geometry; the forward and backward parts are called end-caps and the central region is called a barrel. The detector is supported with new critical components, a Vertex detector to provide a better resolution ($\approx 50\ \mu m$) for particle tracking and cover a larger solid angle. A central tracking chamber, a time-of-propagation chamber, and an aerogel ring-imaging Cherenkov detector are re-built. These new components are discussed in some detail below.

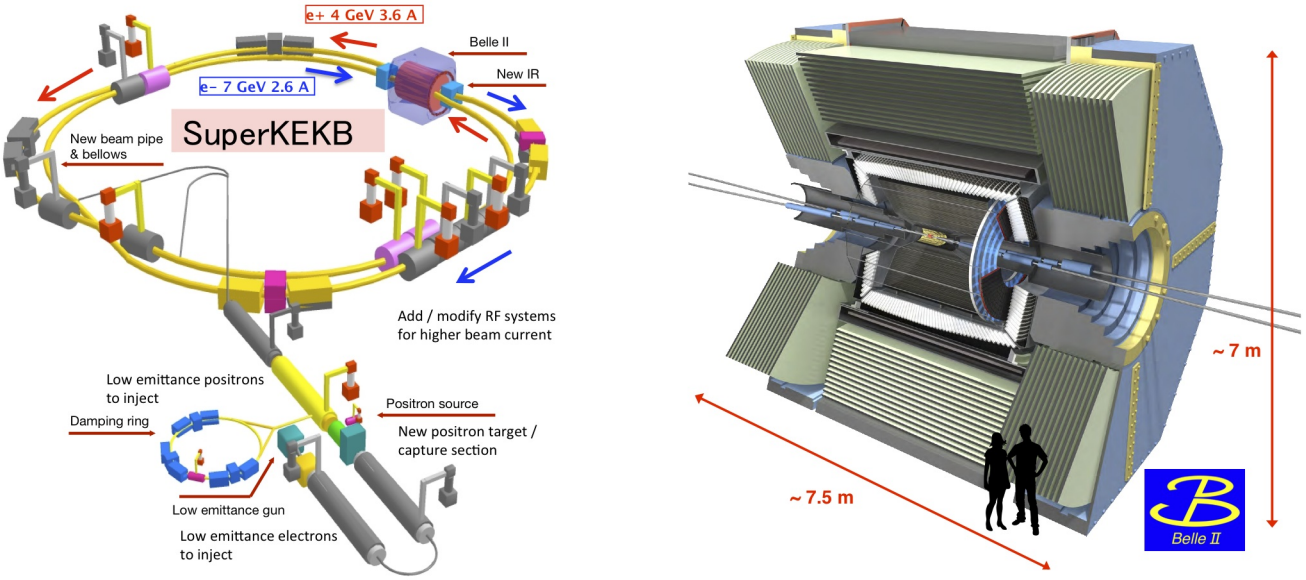

Figure 2: SuperKEKB-Belle II Detector

3.1 Vertex detector (VXD).

- **Structure**: In fig5, the innermost layer(a pixel detector (PXD) followed by a silicon vertex detector (SVD)) are together composing the vertex detector (VXD).
  The (PXD consists of two layers at 14 mm and 22 mm from the interaction point. In the innermost layer, every single pixel has a dimension of $50\times50-55\mu m$ and $50\times70-80\mu m$ for the outermost layer.The PXD is based on the DEPleted Field Effect Transistor (DEPFET) technology. Charged particles traversing the semiconductor material create electron whole pairs which drift to oppositely charged areas in the pixel, generating a voltage which can be measured, digitized and further transmitted tot he data acquisition (DAQ) system.
  silicon vertex detector (SVD), contains four layers of double-sided silicon strip sensors (DSSDs) at radii of 38 mm, 80 mm, 115 mm, and 140 mm from the interaction point. Four layers are made of several ladders which overlap with the adjacent sensor's area to

cover the whole plane.

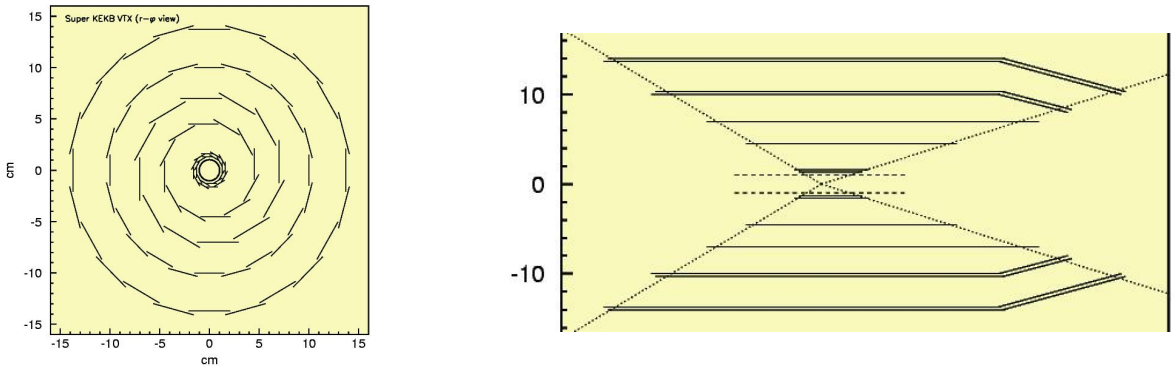

Figure 3: Belle II Vertex Detector with two pixelated layers and four layers with silicon strip sensors around a 10 mm radius Be beam pipe.

- **Purpose**: As the first two layers and the Be beam pipe are closer to the interaction point, this provides better resolution for particle tracking. The outermost layer is a bigger radius which will cover a larger solid angle from 17 to 150 degrees and allow for the best reconstruction of the position of low-momentum particles that may not reach the outer tracking detector.

3.2 Central Drift Chamber (CDC)

- **Structure**: CDC detector is the third component after the VDX detector from the IP and extends to a larger radius of 1130 mm and comprises nearly 14 336 sense wires grouped in 56 layers. The CDC is divided into 9 super-layers which alternate either in "axial" or "stereo" orientation. The CDC chamber is filled with an equal proportion 50:50 mixture of gas $He - C_2H_4$ and immersed in a high magnetic field of 1.5 T provided by a superconducting solenoid magnet. When a particle beam interacts with the gas molecules, it creates positive ions and electron pairs, which consequently have enough kinetic energy ionize other gas atoms and thus creating an avalanche of electron hole pairs. CDC uses an electric field between the wires, so the electrons are attracted to the anode which then transmits to the sense wires to produce the signal. The average drift velocity and the drift time provide information on incident particle position, these positions make up the trajectory of the particle.

- **Purpose**: CDC is dedicated to reconstructing charged tracks and estimates their momentum precisely from the bending radius that creates from the motion of charged particles in the magnetic field. From this relation $\frac{p}{e} = B\rho$, one calculates the momentum p, where e is the electron charge, B is the magnetic field and ρ is the bending radius. As CDC is a gaseous Detector, the particle energy loss $\frac{dE}{dx}$, calculated from Bethe-Bloch Formula, can provide an input for particle identification. Also, one of the important roles of the CDC is recording efficient and reliable trigger signals for charged particles.

3.3 Particle Identification Detector

- **Detection principle**: Particle Identification Detector splitting into two sub-detectors,

an Aerogel Ring Imaging Cherenkov (ARICH) counter and Time of propagation (TOP) counter. Both share the same detection principle, based on the Cherenkov effect: Which occurs when a charged particle goes at a speed higher than the speed of light in a medium, [1], in a cone shape, as shown in fig4. The opening angle of the cone along the direction of the particle trajectory is,

$$\cos\theta = \frac{1}{\beta n} \tag{9}$$

Where n is the refractive index and $\beta = v/c$ is the relative velocity, v is the velocity of the particle, and c is the speed of light.

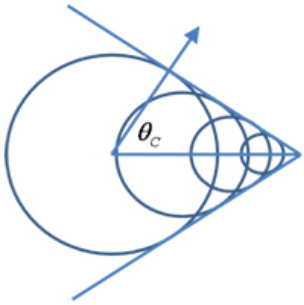

Figure 4: Cerenkov radiation effect

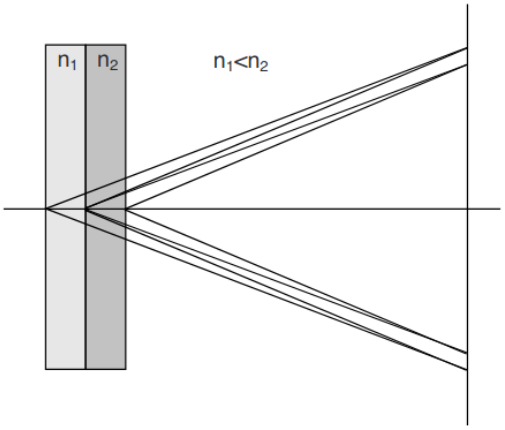

Figure 5: The focusing configuration of ARICH detector.

3.3.1 ARICH - Particle Identification Detector

- **Structure**:A proximity-focusing Aerogel Ring Imaging Cherenkov (ARICH) counter, fig5, is one of the identification systems used at the forward end-cap of Belle II. It is comprised of two layers of 2 cm thickness of a non-homogeneous aerogel with different refractive indices (n = 1.045, n = 1.055), in order to increase the number of detected Cherenkov photons. The Cherenkov light comes from the aerogel detector and expands to form a ring in the photon detector located 20 cm from the radiator. An array of Hybrid Avalance Photo-Detectors (HAPD) cause the photons of the aerogel ring to free electrons in their sensitive area, which accelerate in an electric field and cause an electron avalanche for amplification.

- **Purpose**: ARICH detector is able to separate pions and kaons in the momentum region from 0.4 to 4 GeV/c. As it is sensitive to the angle of Cherenkov light emission, thus the particle velocity can be measured for particle identification.

[1]Nothing can move faster than light in a vacuum but in water, the speed of light is only 3/4 of its speed in a vacuum

3.3.2 TOP - Time Of Propagation Counter

- **Structure**: Another particle detector for particle identification is Time of propagation, which surrounding the CDC, and consists of a photon detector system at the backward side and synthetic quartz radiators(2.6 m long and with size $2700mm \times 450mm \times 20mm$). In fig6, the incident charged particle travel along the quartz radiator (n=1.55), and Cherenkov light is reflected by a focusing mirror by repeating total internal reflection on one end and measured by PMTs on one edge of the detector. In a region between the photon detector and the radiator bar, a prism is employed to expand Cherenkov radiation rings in front of the photon detectors. The TOP counters used in Belle II are in total 16 and each plate is composed of a 45 cm wide and 2 cm quartz plate.

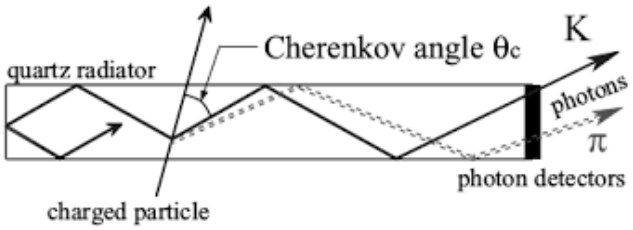

Figure 6: Belle II TOP Detector

- **Purpose**:As TOP counter uses photo-sensors, it provides a good timing resolution in the range of 100 ps (achieved with a 16-channel MCP PMT) which consequently allows reconstructing Cherenkov ring images by estimating the arrival time of flight of each Cherenkov photon. Hence, the separation of particles is achieved according to their momentum.

3.4 Electromagnetic Calorimeter (ECL)

- **Structure**: A calorimeter measures a particle's energy by measuring the radiation length (X_0) of the charged particle in a material, as shown in fig7. ECL is appropriate for observing the electromagnetic shower that are produced as final daughters of B meson decay such as photons and electrons. It is placed between the solenoid of the magnet and the TOP counter and consists of a highly-segmented array of thallium-doped with cesium iodide CsI(Tl) crystals, in total 8736 crystals used with attached preamplifiers and readout electronics. Each crystal has a tapered shape of 30 cm in length and an average size of about 6×6 cm^2.

- **Purpose**: The main important role of the Electromagnetic Calorimeter is detecting photons with high efficiency and accurate determination of photon energy and its directions, as well as electron identification from other charged particles based on the ratio of energy deposit to the momentum. Since the interesting trigger lines for this analysis are the lml trigger lines, which are mainly provided by the ECL, will be discussed in some detail in the data analysis section.

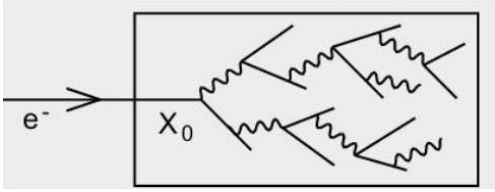

Figure 7: Sketch of shower development ECL

3.5 K_L^0 - Muon Detector (KLM)

- **Structure**: KLM detector consists of alternating iron plates and detection material, placed outside the superconducting solenoid coil. KLM covers an azimuthal angle $20^o < \theta < 150^o$ and it splits into the barrel part (BKLM), aligned parallel to the beam, and end-cap region (EKLM), aligned normal to the beam. The barrel part has an octagonal shape, consisting of 14 iron-plate layers and 15 detector layers. The two end-caps have 14 detector layers and 14 iron plates.

- **Purpose**: The critical function of the KLM detector is to observe K_L^0 and μ particles. K_L^0 mesons interact hadronically with Iron plates, while muons are leptons that undergo electromagnetic interactions. One can notice that pions and muons have almost the same mass and in order to identify a muon from a pion, we must take into account the nature of the interaction with a matter where muons interact with material only by ionization, while pions interact by strong interaction and thus most of the hadrons stop in the iron plates, and muons pass-through the iron plates of KLM if it has enough high Energy.

4 Lepton Flavor Violation

The lepton falvor is, apart from neutrino oscillations, a conserved quantity in the SM. Investigating Lepton Flavor Violating (LFV) decays, such as $\tau^{\pm} \to l^{\pm} K_s^0$, might hint for new physics outside the SM, which is one of the research topics of the Belle II experiment. Due to the large taupair data set, the experiment will accumulate over the next years, the branching fraction of some LFV decays might become accessible [9],[10].

4.1 The Standard Model and Lepton Flavor Violation

The standard model of elementary particles explains the fundamental forces (electromagnetic, weak, strong interactions) and classifies all known elementary particles constituents. So far it has successfully explained almost all experimental results, precisely. SM introduces several classes of elementary particles and distinguishes them by other characteristics such as spin, charge, color charge, and so on. It includes 12 elementary particles called fermions with spin $\frac{1}{2}$ and four gauge-bosons with spin 1, which mediate the forces and the higgs boson generating the masses of particles. Fermions are classified into two groups according to their interaction with matter; 6 quarks (up, down, charm, strange, top, bottom) which interact via all 3 forces. Charged leptons (electron, muon, tau) interacting via electromagnetic and weak force and (electron neutrino, muon neutrino, tau neutrino) interact by weak force only. Quarks and leptons

are arranged into pairs according to similar physical behavior, named family or generation, the most stable particles belong to the first generation and the less stable or heavier ones make up the second and third generations. The force carriers are mediated by gauge bosons with a spin 1, that is, the 8 gluons mediate the strong interaction between quarks, the $W^{\pm}, Z^{0}$ gauge bosons mediate the weak interactions and Photons mediate the electromagnetic force. Unstable particles decay into lighter ones and this governs by:

Nother's theorem: reveals that each symmetry in nature leads to a conservation law and vice versa. For example, the invariance under translation in space leads to momentum conservation, and invariance under translation in time leads to energy conservation. SM explains Lepton Flavor Violation in the absence of neutrino mass, considering it equal to zero, by assuming the lepton number in the initial and final state must be equal. For instance, leptonic numbers $L_{e^-} = +1$, $L_{\mu^-} = +1$ and $L_{\tau^-} = +1$ and to the corresponding antiparticle doublets (e^+ , $\bar{\nu}_e$), (μ^+ , $\bar{\nu}_\mu$) and (τ^+ , $\bar{\nu}_\tau$) respectively the numbers L_{e^+}= -1, L_{μ^+} = -1 and L_{τ^+} = -1 and these numbers are always conserved separately.

But the neutrino oscillations phenomenon indicates that the neutrino of one flavor mix and transforms into another which means, the neutrinos have masses and the lepton family quantum numbers are not conserved. Hence, LFV processes occur in nature and that makes SM unsatisfactory and needs generalization.

4.2 Lepton Flavor Violation Beyond the Standard Model

The super-symmetry, seesaw mechanism, and scalar leptoquark Yukawa couplings are physics models that predicted the branching ratios of lepton decays in the charged sector. In this section, a brief definition of these models will be introduced.

- **Seesaw Mechanism:** This model is used to generate neutrino masses to SM. It assumes the neutrino mass has a left-handed mass(Dirac mass) of 1 eV and a right-handed Majorana mass of $10^6 GeV$. This difference in masses leads to the dynamics of this process being very small of a branching ratio of less than 10^{-40} which is inaccessible with current experiments. SM with seesaw results in a failure to produce observable charged lepton flavor violating rates, thus a $\mathbf{super-symmetry}$ model is considered as another extension for SM. It assumed that bosons and fermions by relating them equivalently by transformations $Q\,|F\rangle = |S\rangle$. In other words, each fermion has a SUSY boson partner and vice versa. For example, tau particle, there is a superpartner particle with the same charge and mass but with a spin of 0.

For instance, Super-symmetry with a seesaw mechanism consider the mediator of *tau* decay modes is Higgs boson. In this case, the predicted branching ratio less than 10^{-7} for ($\tau \to 3\mu$) and 10^{-10} for ($\tau \to \mu\gamma$) which considered the largest predicted branching ratio in τ LFV.

- **LeptoQuark Model:** is still studied at LHC to explain violation of lepton flavor universality, and some assumptions are proposed to describe LeptoQuark (LQ) hypothetical particle: as an electrically charged gauge boson, which couple to a quark and a lepton, and carrying both baryon number (B) and lepton number(L). The spin state of leptoquark is assumed to be a vector bosons of spin 1 and scalar bosons of spin 0. The feynman diagram for a scaler boson is displayed in Fig8.

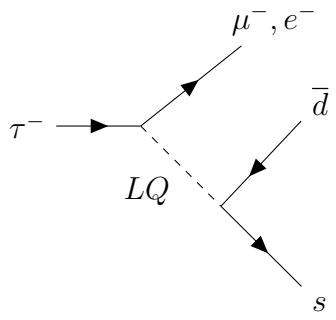

Figure 8: Feynman diagrams for the processes $\tau^- \to l^- K_s^0$

BaBar and Belle experiments, using 469 and 671 fb^{-1} of data, respectively, present the upper limits at confident level 90% for $\tau^- \to l^- K_s^0$ decay modes as in Table 1.
Belle II experiment might be able to use 50 ab^{-1} of data, and since $BR \propto 1/\sqrt{L}$, one expect an improvement in BR with the integral luminosity compare to the other experiments.
In this report, we represent the search for $\tau^- \to l^- K_s^0$ decay of a branching fraction, defined as:

$$B_{UL}^{90}(\tau \to l K_s^0) = \frac{s^{90}}{2.\mathcal{L}.\sigma_{\tau\bar{\tau}}.\epsilon_{lK_s^0}} \tag{10}$$

Where s^{90} is the upper limit of 90% confident level on the signal yield, $\mathcal{L}$ is the integrated luminosity, $\sigma_{\tau\bar{\tau}}$ is the cross section of taupair production and $\epsilon_{lK_s^0}$ the signal efficiency.

Experiment	$B_{UL}^{90}(\tau^- \to e^- K_s^0)$	$B_{UL}^{90}(\tau^- \to \mu^- K_s^0)$
BaBar obs.	3.3×10^{-8}	4.0×10^{-8}
Belle obs.	2.6×10^{-8}	2.3×10^{-8}

Table 1: upper limits obtained by BaBar and Belle

4.3 Motivation for $\tau^- \to l^- K_s^0$

As the tau lepton has the heaviest mass among the leptons, it can decay to many hadronic modes and has many possible τ LFV modes which could couple to NP.
With updated analysis methods, such as Boosted Decision Trees (BDT) and an upcoming large taupair data set of Belle II, the branching fraction of this channel might be in the vicinity of the experimental boundaries.

4.4 Search Strategy

The method used to search for any LFV decay is followed by the separation of an event into two hemispheres according to the thrust axis which is defined as the axis that maximizes the sum of all the particles' momenta projections onto it.
We search for $\tau^+\tau^-$ that includes two decay sides. One τ (tag side) decays into charged particles and additional neutral particles, neutrinos, or photons. The other τ (signal side) decays into $l^- K_s^0$ or $l^- K_s^0 K_s^0$, this part is LFV mode and under study. The schematic fig9 shows the decay kinematics separation, the ϕ angle around the detector and perpendicular to the electron beam, and θ angle is running in the beam direction from 17^o and 150^o. This analysis aims for

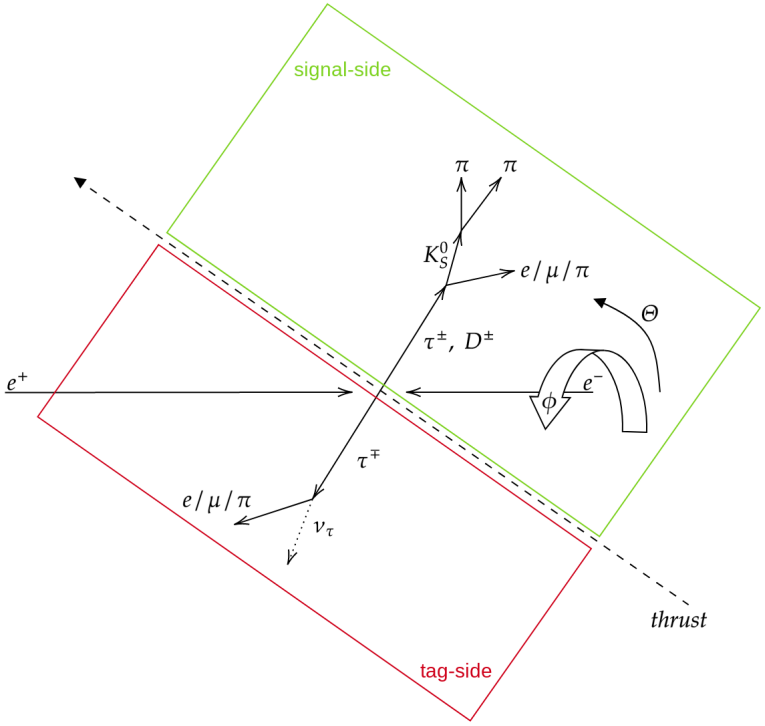

Figure 9: schematic of the τ decay kinematics(signal side and tag side) with respect to the thrust axis.

a branching fraction upper calculation and thus is crucially dependent on the signal efficiency and remaining background events. A set of one dimensional selections to reduce background is applied, before the remaining events undergo a BDT selection, which aims at reducing the background to 0, by keeping a high signal reconstruction efficiency.

5 Data Analysis

The main purpose of this analysis is to make a comparison between the data and Monto Carlo samples in the signal channel $\tau^\pm \to l^\pm K_s^0$ sidebands, as well as for a reference channel. The reference channel in this analysis is the decay of $D^\pm \to K_s^0\pi^\pm$ which has a similar decay kinematics as the $\tau^\pm \to l^\pm K_s^0$ signal channel. This section will discuss the description of particle reconstruction. Firstly, Event Selection for the Monto Carlo simulation. Secondly, the trigger system at Belle II and the implementation of the trigger efficiency correction for real data and simulated MC data. Finally, the study of the signal channel sidebands will be introduced.

5.1 Signal and Background

This part will discuss the signal selection performed for $D^\pm \to K_s^0\pi^\pm$ (Reference channel), and MC background. The term background is refers to the standard model physics processes, as well as the beam-beam interactions and interactions of particles with the detector material all simulated in MC. the non physics background can be classified into two types, beam-induced process, and luminosity-dependent process. **beam induced process** is generated from the collisions of beam particles with the gas beampipe leading to Beam-gas scattering and the Tou-

schek effect. While **luminosity dependent process** originate from electron-positron collisions resulting in Radiative Bhabha and Two-photon process. These different types of backgrounds are presented below:

- **Beam-gas scattering**: The incoming beams can interact with residual gas molecules in the beampipe leading to coulomb scattering which changes the beam particles' direction; and Bremsstrahlung which reduces the beam energy.
- **Touschek effect**: It is a Coulomb scattering interaction between particles in the same bunch in a storage ring, and one of the main effects causing beam background. Since it is proportional to the inverse beam-size, it is increasing with the squeezing of the beams towards the design luminosity. This effect may occur at the interaction point and nearby the detector makes a shower of particles that may be collected by the detector components.
- **Radiative Bhabha**: It refers to the electron and positron interaction where the particles do not annihilate, but scatter and emit several photons during the process. These are crossing the beam pipe under small angles and convert to secondary particles.
- **Two photon process**: An electron-positron pair is produced with low momentum from $e^-e^+ \rightarrow e^-e^+e^-e^+$ which then will spiral around the magnetic field creating a small synchrotron radius, and leave a lot of hits.

5.1.1 Data samples

In this analysis, MC simulation produced by the Belle II data production, corresponding to an integrated luminosity of 200 fb^{-1} and the real data is corresponding to 189.9 fb^{-1}. MC data is splitting into a signal and background. MC background is composed of a part coming from Υ(4S) resonance, which is $B\bar{B}$, $B^0\bar{B}^0$ and $\tau\bar{\tau}$, $q\bar{q}$ (q=u,d,s,c), $\mu\bar{\mu}$. A list of the samples in use and the corresponding luminosities can be seen in Table2,

Process	Integrated luminosity
$e^+e^- \rightarrow \tau^+\tau^-$	6000 fb^{-1}
$e^+e^- \rightarrow u\bar{u}$	6000 fb^{-1}
$e^+e^- \rightarrow d\bar{d}$	6000 fb^{-1}
$e^+e^- \rightarrow s\bar{s}$	6000 fb^{-1}
$e^+e^- \rightarrow c\bar{c}$	6000 fb^{-1}
$e^+e^- \rightarrow B\bar{B}$	1000 fb^{-1}
$e^+e^- \rightarrow e^+e^-\gamma$	50 fb^{-1}
$e^+e^- \rightarrow \mu^+\mu^-$	1000 fb^{-1}
$e^+e^- \rightarrow e^+e^-e^+e^-$	200 fb^{-1}
$e^+e^- \rightarrow e^+e^-\mu^+\mu^-$	200fb^{-1}
$e^+e^- \rightarrow e^+e^-\pi^+\pi^-$	1000 fb^{-1}
$e^+e^- \rightarrow e^+e^-K^+K^-$	2000 fb^{-1}
$e^+e^- \rightarrow e^+e^-p^+p^-$	2000 fb^{-1}

Table 2: Event type and luminosity for the background MC in use.

As a first step in the comparison analysis of data and MC, one must examine the number of events in both real data and MC data frames when plotting a Histogram for both data frames. Usually, **Real Data** uses weight 1 but **MC data frame** is unweighted and need to use weights [2]. To illustrate this point, the number of events generated by the Monto Carlo simulation is not equivalent to the number of events we expect in real data. So in order to create MC plots with our expectation of what to see in real data, one needs to apply some weights to MC data frames as,

- MC (event weight of data) = MC (event weight)$\times \frac{L_{data}}{L_{MC}}$

L_{data} and L_{MC} are the integrated luminosity of the real data (189.9 fb^{-1}) and MC sample(200 fb^{-1}), respectively. In the fig10 and 11, it shows the total number of events becomes closer to the actual number of MC events expected in data.

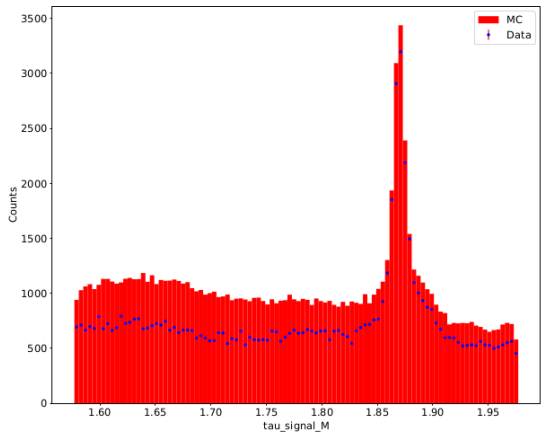

Figure 10: Weighted MC data frames for tau-signal-M variable

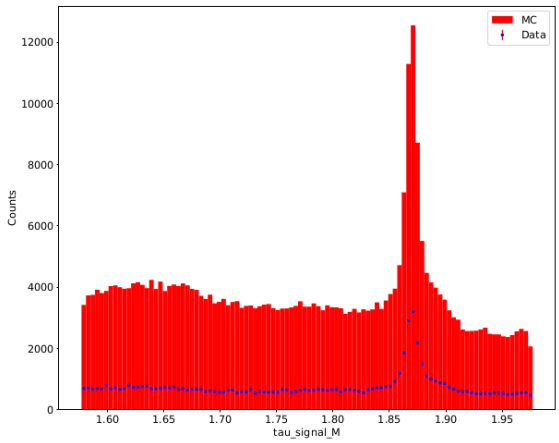

Figure 11: Unweighted MC data frames for tau-signal-M variable

The ratio between real data(X) and MC simulated data frames(Y) is calculated through the error propagation(σ_R) formula as:

$$\sigma_R = \frac{X}{Y}\sqrt{\frac{1}{X} + \frac{1}{Y}} \tag{11}$$

Where σ_x and σ_y are the uncertainty in data and MC respectively. The following plots in 12 represents the data(error-bars) and MC (hatched) ratio.

[2] which is defined as the internal weighting of the different background processes.

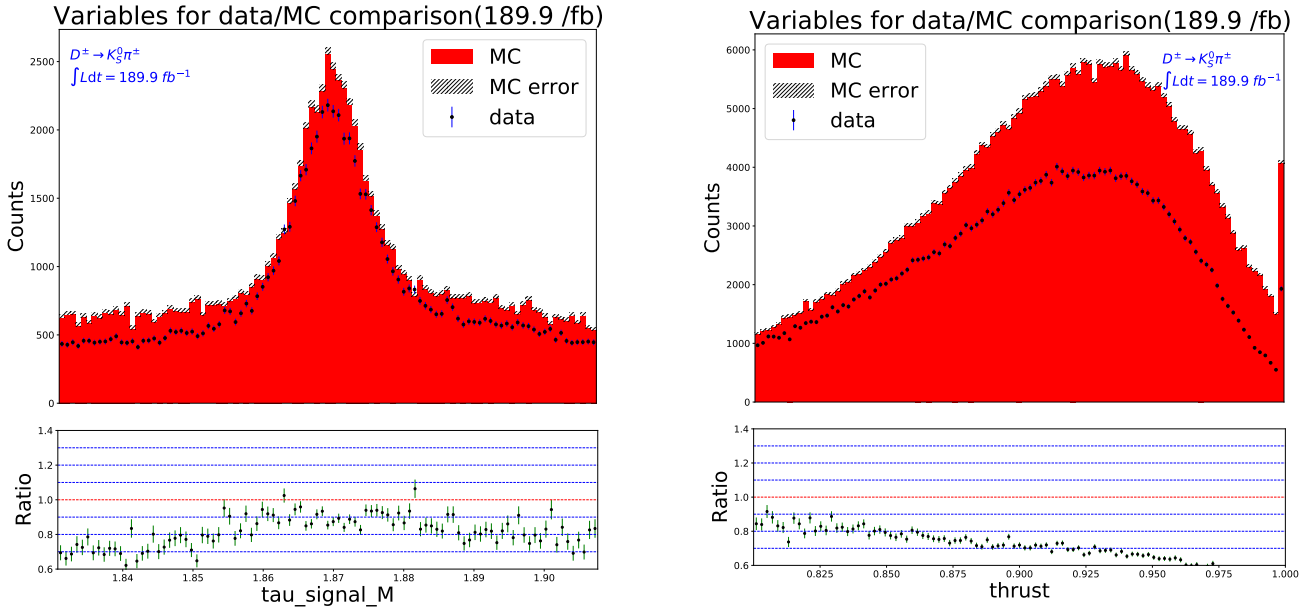

Figure 12: Data/MC agreement for $D^{\pm} \to K^0_s \pi^{\pm}$ reference channel.

5.1.2 Event Selection

After weighing data and MC, we split MC data into signal and background which performed as,

- **Signal(Reference Channel)**: In the reference channel, the signal is defined as $D^{\pm} \to K^0_s \pi^{\pm}$. To be sure, that the signal is correctly reconstructed, MC truth matching information is used. Thus, all participating particles are required to have a matching PDG particle ID and the daughter particles are required to originate from the corresponding mother. Two pions originating from a K^0_s and the K^0_s, as well as the additional pion originating from a D meson. the decay of $K^0_s \to \pi^{\pm}$ is reconstructed by combining charged pions, which originate from the mother K^0_s, that have an invariant mass 450 $MeV/c^2 < M_{\pi^{\pm}} < 550\ MeV/c^2$.

- **MC background:** is splitting into sub-MC data, in other words, there are various sources that produce the background as mentioned above. The total MC is considered as the sum of all different types of background and MC signal. In the sample used in this analysis, most of the background events from $q\bar{q}$ and from low multiplicity.

The reference channel candidates in this analysis selected by PDG (Particle Data Group) codes as,

∗ abs(lepton signal mcPDG) equals:

- $e^{\pm} == 11$
- $\mu^{\pm} == 13$
- $\pi^{\pm} == 211$

∗ abs(tau signal mcPDG) equals:

- $D^{\pm} == 411$ (for the reference channel) with
  abs(K_s^0 signal genMotherPDG)==411 and abs(lepton signal genMotherPDG)==411
- $\tau^{\pm} == 15$

* K_s^0 signal mcPDG == 310 with
  abs(pion1 signal genMotherPDG)==310 and abs(pion2 signal genMotherPDG)==310
* abs(pion1 signalmcPDG) == 211
* abs(pion2 signal mcPDG) == 211

The stacked histogram for the reference channel and backgrounds is plotted as shown in fig 13. The plots in Fig13 and 14 show the data to MC agreement on the mass of the reconstructed D meson, which we use as reference channel. Fig. 13 shows the mass over the full range. As can be seen, the data/MC comparison is better in the vicinity of the D mass peak. That is why all further comparison is done in the $1.83 < M_D < 1.91$ mass window, as is shown in Fig. 14. As shown in the plots, for better comparison, the data/MC needs some corrections so that a trigger lines are applied to the analysis as will see in the next section.

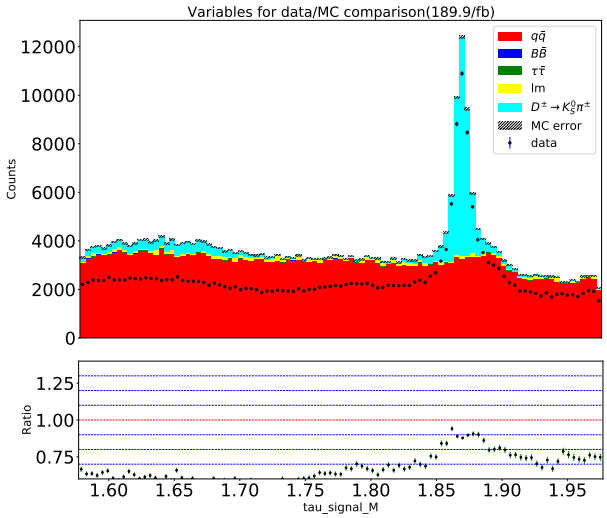

Figure 13: Stacked plot for data and MC backgrounds

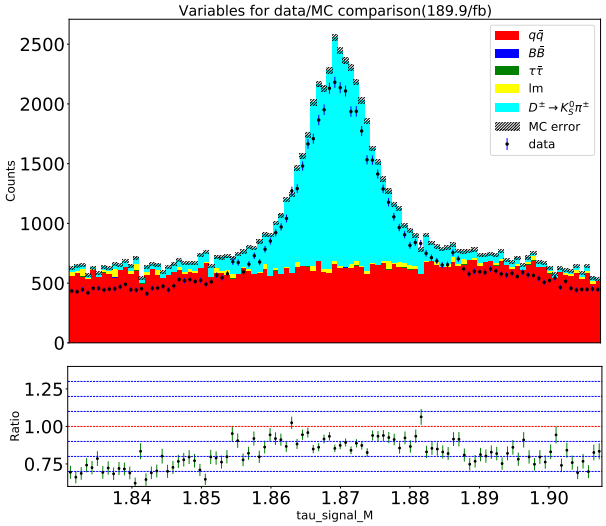

Figure 14: Stacked plot for data and MC backgrounds in mass window $1.83076 < M_\tau < 1.90762$

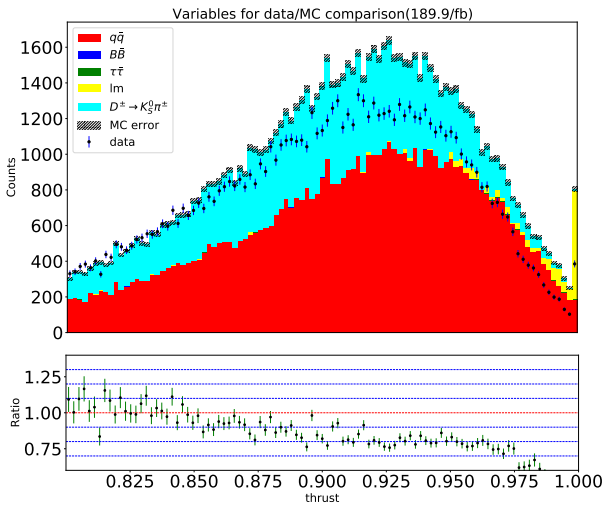

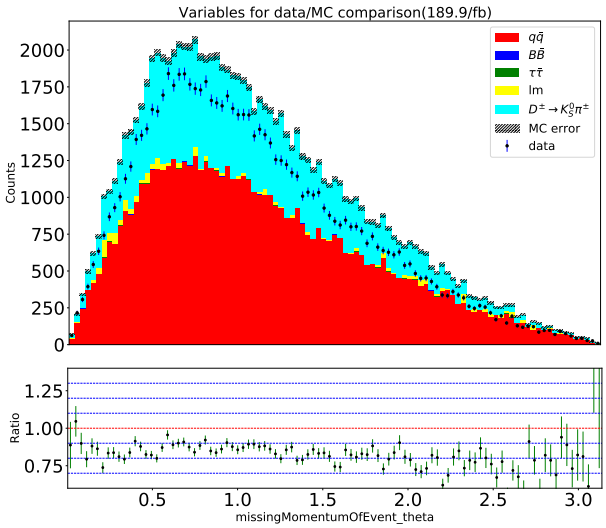

6 Trigger system

The trigger system at the Belle II experiment has a significant role in recording and processing physics events. As concerned, in the Belle II detector section, the sub-detectors are developed for particle identifications and tracking in which particular signatures are observed. Firstly, the triggering system comprises five sub-triggers activated by the signals input of the sub-detectors. Each sub-trigger contains parameters associated with the interesting events such as the number of tracks, total energy deposit, and polar angle of tracks. These sub-trigger hits are transmitted to the Global Decision Logic (GDL) to select if the event must be recorded or rejected. Finally, The data acquisition system receives the trigger signals from GDL to store the data that obey the trigger conditions, otherwise, the event data will not be considered. There are many trigger lines which are processed by the GDL and attached to as event variable to the data. For MC,

a dedicated trigger simulation is simulating the trigger response to a reconstructed event and also attaches it to the MC data. In this section the trigger lines, which are important for this analysis, will be discussed.

6.1 Trigger selection to the data and MC data-frames

In the following work, the selection of trigger lines in our data frames are focusing on, **low-multiplicity trigger lml** that are all based upon ECL information, and looks like this:

- lml trg = (lml0==1 or lml1==1 or lml2==1 or lml4==1 or lml6==1 or lml7==1 or lml8==1 or lml9==1 or lml10==1 or lml12==1 or lml13==1).

The link with **Or** between each line is corresponding to which line is fired for an event, that contains all information required, so that we keep this event. And **orthogonal trigger CDC**, which selected as:

- cdc trg = (fff==1 or ffo==1 or ffy==1 or ffs==1)

Orthogonal lines mean that the event is fired by independent signatures, and no trigger information is used for the lml and CDC triggers, in other words, CDC is used as a reference trigger to measure lml trigger efficiency.

Since the trigger in case of data is coming from the individual sub-detectors of the experiment and the trigger used for MC is simulated, a trigger efficiency correction for the data/MC comparison needs to be applied. This will be the topic of the next section.

6.2 Correcting for the trigger efficiency

The goal of this part is to correct the different trigger efficiencies in data and MC. First, we measure the trigger efficiency for data and MC separately as follow: by selecting all events, which fired one of our trigger lines of interest (the lml trigger lines) and compare that with the number of events where an orthogonal trigger line was fired, which can be calculated from the relative trigger efficiency as:

$$\epsilon_{rel} = \frac{trg(lml) \cap trg(CDC)}{trg(CDC)} \tag{12}$$

ϵ_{rel} is defined as the probability of an event to be selected, with a number of some conditions related to the trigger lines such as (number of tracks, energy, mass, momentum, etc.)
In figures 15, 16, do NOT show the data/MC comparison after trigger correction. They show in different colors the events which are left in data (errorbars) and MC (histogram) after the lml, lml and CDC and CDC trigger selection. In the inset plot the trigger efficiency for data (errorbars) and MC (histogram), as well as the ratio of data trigger efficiency over MC trigger efficiency (which we want to correct for) is shown.

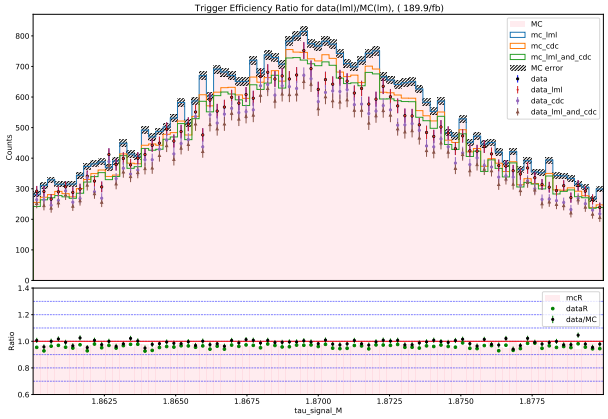

Figure 15: Data/MC comparison with trigger lines for tau signal M variable

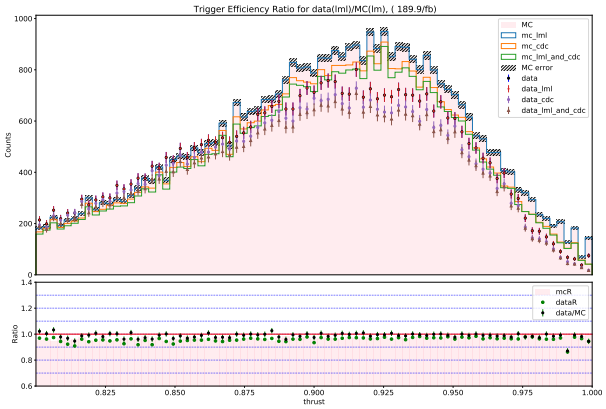

Figure 16: Data/MC comparison with trigger lines for thrust variable

6.2.1 Implement trigger efficiency correction for data/MC

The trigger efficiency ratio is applied bin-by-bin as a ratio of the trigger efficiency on data divided by the trigger efficiency on MC, by measuring the $\epsilon_(rel)$ for data and MC and then calculating the trigger efficiency ratio ϵ in each bin as:

$$\epsilon = \frac{\epsilon_{rel(data)}}{\epsilon_{rel(MC)}} \tag{13}$$

The above mentioned ratio is now applied to the MC distribution for each bin as a correction factor multiplied to the bin entries. Finally, the implementation is done and the data/MC comparison is performed for all 35 variables again with both: the measured bin-by-bin trigger efficiency correction and the trigger selection trg(lml). One notice in the plots below 17, that the correction is small (about 1%) and the comparison still need other corrections to reach a better agreement.

7 Study for the signal channel $\tau^{\pm} \to l^{\pm} K_s^0$

In this section the online reconstruction, for the signal decay $\tau^{\pm} \to l^{\pm} K_s^0$ is discussed and the data and MC samples used for the data to MC comparison are introduced.

- **Data** used in this analysis is with integrated luminosity $189.9 fb^{-1}$ and the MC data frames used $\int \mathcal{L} = 2ab^{-1}$.
- **Signal Monte Carlo Simulation** sample, we use generic and low multiplicity samples from Belle II MC campaign. These samples are produced with basf2 (Belle II analysis framework) release-05-02-00, for $\tau^{\pm} \to e^{\pm} K_s^0$ generated with TauolaBelleII, including beam background.

The signal candidates of this analysis are also based on the PDG codes as following:

- abs(tau signal mcPDG) == 15

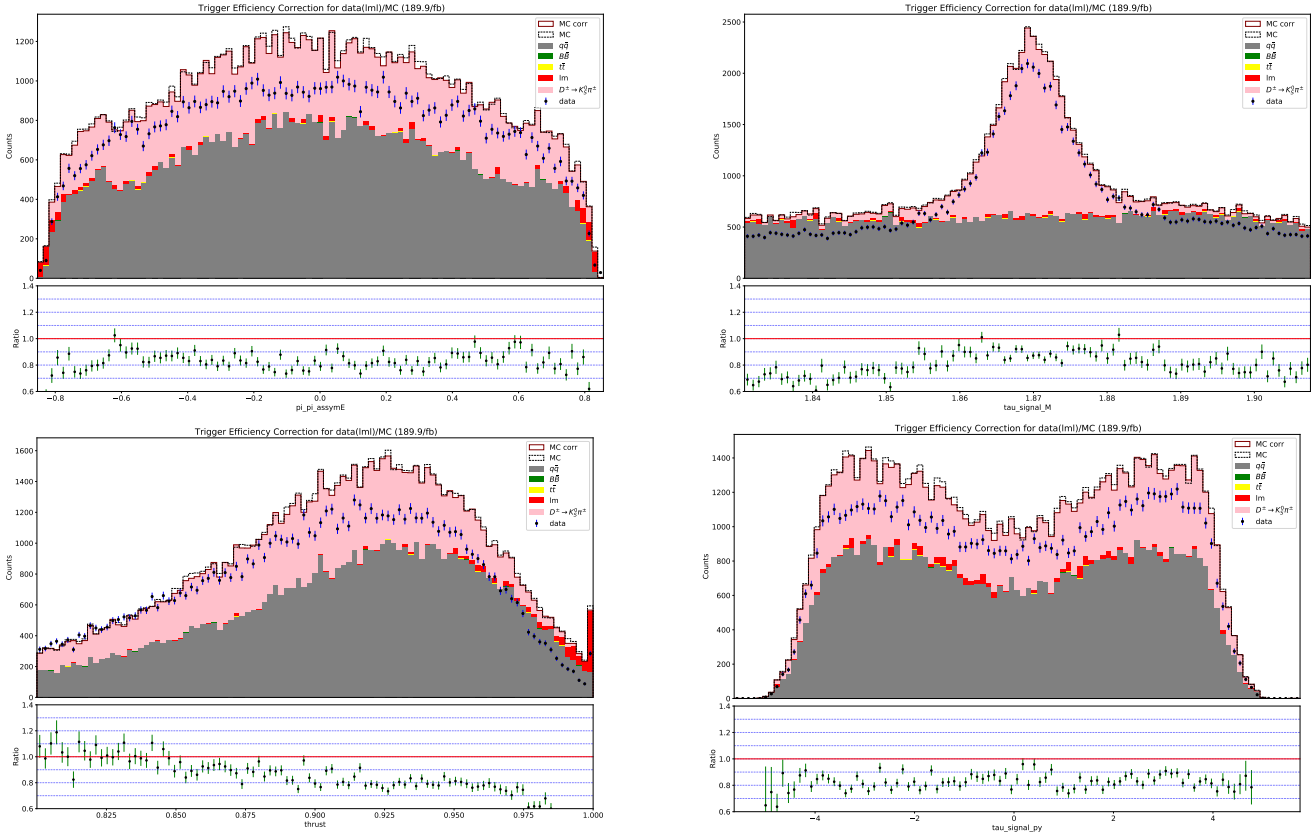

Figure 17: Trigger efficiency correction with trg(lml) for data/MC applied for (pi pi assymE, tau signal M, thrust and tau signal py) variables

- abs(lepton signal mcPDG) == 11 or 13
- abs(K S0 signal mcPDG) == 310
- abs(pion1 signal mcPDG) == 211, abs(pion2 signal mcPDG) == 211
- All daughter particles are required to have a tau ancestor

7.1 Online Reconstruction

Reconstruction is performed with the Belle 2 Analysis Framework (basf2), a modular structured software package written in C++ and steered with python scripts. The data and MC files are provided in ROOT format and are reconstructed event-by-event within the basf2 ring-buffer data storage. During reconstruction the detector information are merged to form for example tracks, calculate deposited energy or provide particle identification. Those quantities are stored in variables which are finally saved to a ROOT file for offline analysis.
As shown in fig 9, the total number of tracks in the event is 7. The signal side(3-prong) consists of a K_s^0 and an electron or muon, with the number of tracks 3. While tag side decays into a final state with a pion, electron or muon track and reconstructed either to one track or 3 tracks. In this subsection, we will introduce the reconstruction parameters used for the selection criteria.

7.1.1 Neutral Particle Selection

- **Photons**: There are 3 list for photons, one is used for calculation of the event shape, another list for photons coming from neutral pions and the last for photons emitted by electrons as Bremsstrahlung. The selection criteria of these photons are performed according to photon energy, polar angle θ as:

  * $E_\gamma > 0.02$
  * $0.8660 < \cos\theta < 0.9563$
  * clusterNHits > 1.5
  * isDaughterOfList(pi0:fromLooseGammas) $== 0$

  For the photons come from neutral pion decays, there are some additional selections are applied, as:

  * $E_\gamma > 0.01$
  * $0.8660 < \cos\theta < 0.9563$
  * clusterNHits > 1.5
  * $0.115 <$ M < 0.152

7.1.2 Final-State Particle Selections

- **Track Selection**: We fill three particle lists for electrons, muons and pions where each candidate has to fullfil the following criteria:

- $\pi^{\pm}, \mu^{\pm}, e^{\pm}$: The electrons, muons and pions candidates must follow these selections:

  * $p_T > 0.1$
  * -3.0 $<$ dz $<$ 3.0
  * dr < 1.0
  * isDescendantOfList(K_s^0:FromLoosePions) $== 0$

Where dz represents the distance between the closest point of the fitted track and the interaction point, dr is the radial distance from the IP, and p_T (transverse momentum) is the projection of the particle momentum in the plane perpendicular to the beam direction. These variables help to reduce the background and achieve precise reconstruction process.
In addition to these selections, other requirements are needed to match with particle identification (pID) variables. In case of **electrons**, we select candidates with electronID > 0.9 and muonID $<= 0.95$. **Muons** are selected with muonID > 0.95 and electronID $<= 0.9$ and **pions** with muonID $<= 0.95$ and electronID $<= 0.9$. Since the hadronID variables are not yet in a optimized, we do not require pionID or kaonID.

- K_s^0 **reconstruction** is performed from the standard K_s^0 particle list, and candidates are required to match with with goodBelleKshort>0, a variable algorithm combining several parameters of the daughter tracks, and significanceOfDistance > 3.

7.1.3 Signal Reconstruction

Reconstruction of τ signal is performed by combining lepton candidates with K_s^0. Also, other selections are taken into account such as:

* At most 6 tracks in the event
* $0.45 < M_{K_s^0} < 0.55$ GeV/c 2
* $1.577 < M_\tau < 1.977$ GeV/c 2
* $1.02253 < \Delta E < 1.01747$ GeV/c

8 Offline Selection

After the online reconstructions, the invariant τ mass and $\Delta E = E_{beam}$ - E_τ distributions of the reconstructed MC truth matched τ events are fitted for electron and muon channel separately, as shown in fig 18. The analysis is performed as blinded analysis to prevent a reconstruction or selection bias towards data events which may populate the 5 σ signal region (SR). Therefore we fit the tau mass and ΔE distributions.

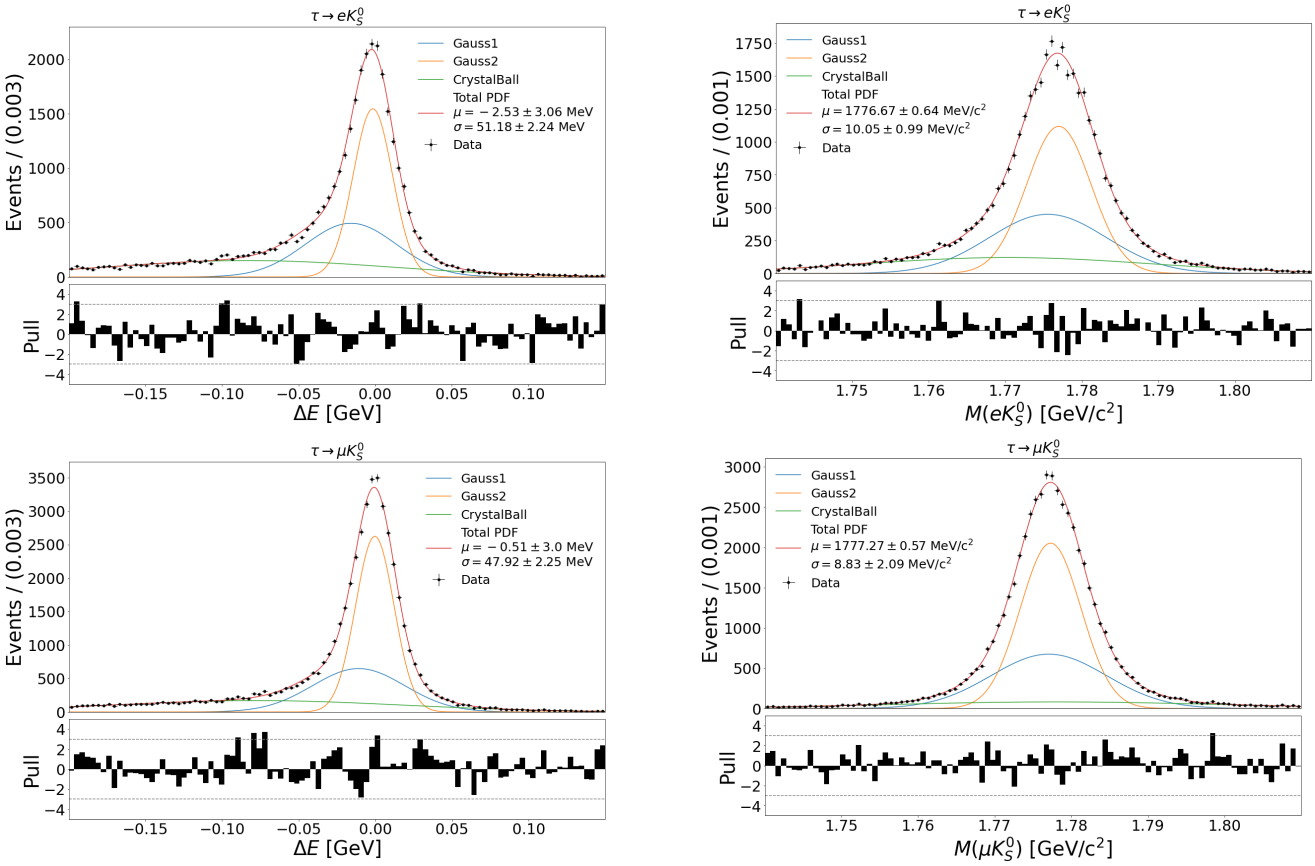

Figure 18: Fits to the mass and ΔE distribution of the reconstructed τ candidates for electron and muon channel.

The important values, which come out of the fit, are μ and σ. μ defines the mean center value of the distribution and σ is the width. In our case, we define the SR as 5 times the width

σ around the mean μ , for both, mass and ΔE. Thus we get a signal region of $[\mu\ (5\ \sigma)/2, \mu + (5\ \sigma)/2]$, which should blinded for data/MC comparison of the signal sample. As seen in fig19, this is a 2D histogram of background and signal, the background is only shown outside the 5 sigma region, while the signal is located in the 5 sigma region in which we define for example the e-channel to be: **'1.727 < tau-signal-M < 1.827 and -0.25753 < tau-signal-DeltaE < 0.25247'**.

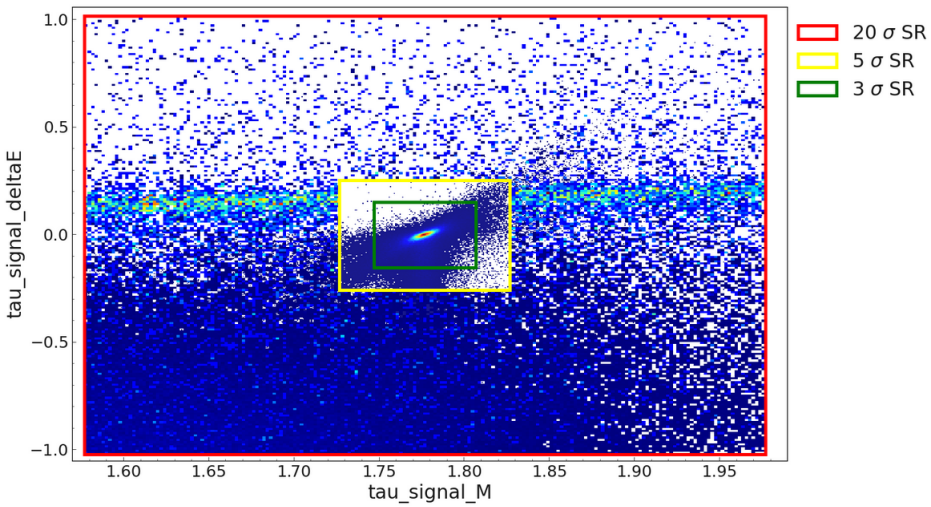

Figure 19: $3\sigma, 5\sigma, 20\sigma$ regions for the electron channel.

8.1 Electron Channel

Other selections criteria are performed for the electron and muon channel in order to increase the signal efficiency and obtain a good signal to background discrimination.
To purify the data and MC samples for the decay, another set of offline selections is applied, which are optimized on MC. For the electron channel the following variables are selected.

- $0.0 < M_e$ tag photons < 6.5
- $0.485 < K_s^0$ signal M < 0.51
- K_s^0 signal flightDistanceErr < 0.6
- -0.98 $< K_s^0$ signal cosHelicityAngleMomentum < 0.98
- track tag E-CMS < 5
- -4 $<$ lepton signal pz-CMS < 4
- M_π tag photons < 1.7

These selections are applied to data ($189.9 fb^{-1}$), MC ($6 ab^{-1}$), and lml trigger selections are applied before. In fig22, tau-signal-mass plot on right, it shows the invariant mass of D meson which reconstructed only for particles coming from the $D^\pm \to K_s^0 \pi^\pm$ decay, this create unique

results for our selections. Also, the signal that we are looking for is visualised as a "peak" in the histogram.

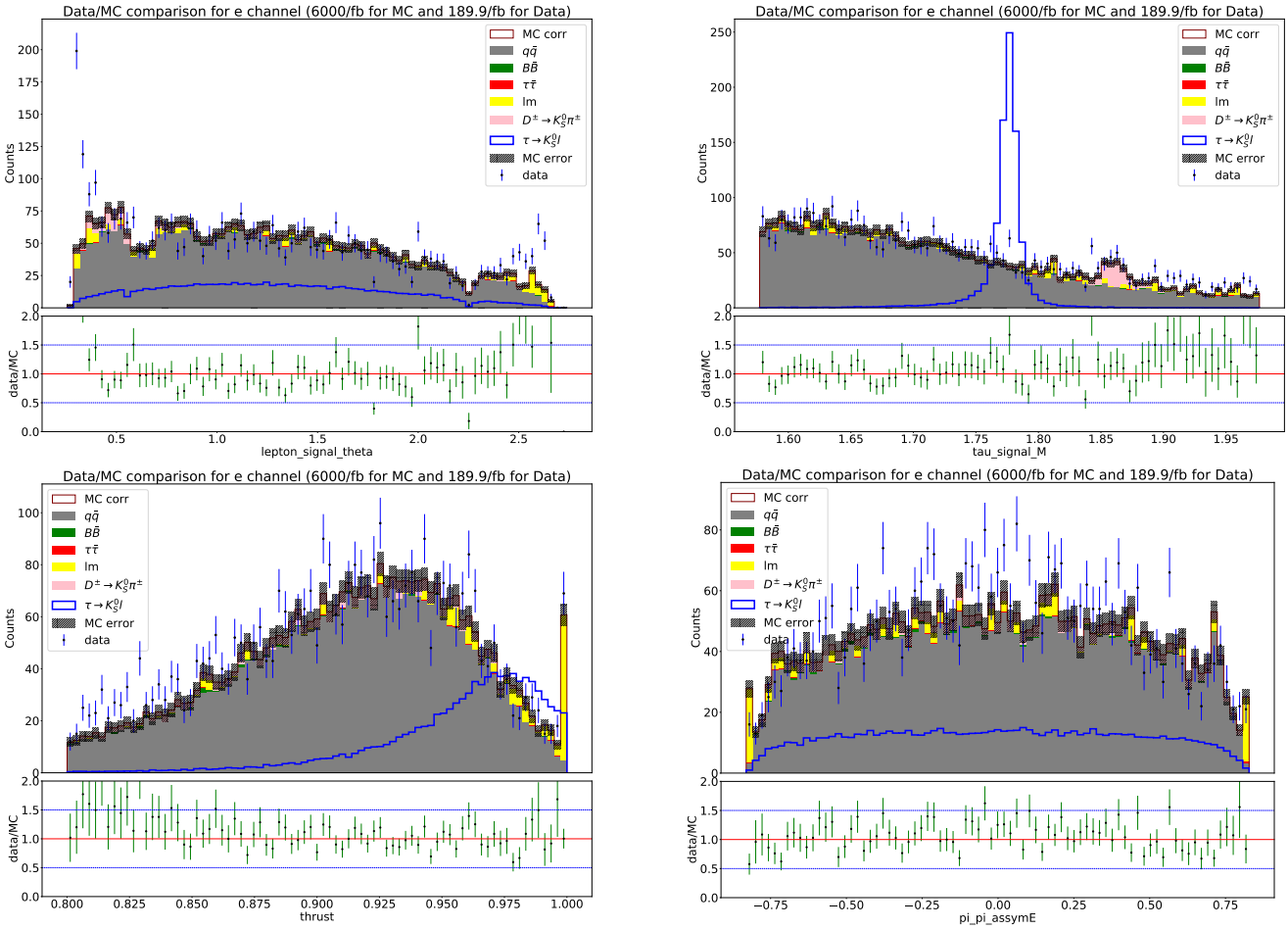

Figure 20: Data/MC comparison after applying electron selections.

- **Additional selection**

The next step in the analysis, is to reduce the number of reconstructed events which make the data/MC comparison less efficient and keep correctly reconstructed events. During the comparison observation of all 53 variables, we notes that the distribution of **lepton signal theta** variable, see fig21, has overshoot data events in two regions we called them low region and high region, that may causes from two photon process or other beam background processes. In our analysis, we split the distribution of lepton signal theta into 3 parts, one for the lower region, one for the higher region and one for the middle region. The lower and high we apply the cut on as following.

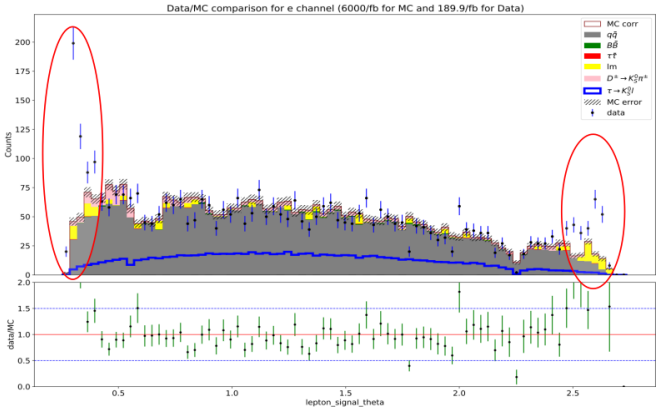

Figure 21: Distribution of lepton signal theta variable.

- **High Region**: $lepton - signal - theta > 2.46$ and,
- **Low Region**: $lepton - signal - theta < 0.4$

In order to reject the overshooting data events in those regions, some selection requirements could be assigned and keep the middle region untouched to check again the agreement of our data frames.
First, we split the tag side into haronic and leptonic, in order to check which variables of the real data are away from the distribution of the signal and not strongly correlated to the M(τ) and Δ E, which are used to define the signal region. and which are not correlated to one of our main variables that used to define the signal region. **Second**, Since we want to find selections reducing the data in the lower and higher regions of **'lepton-signal-theta'**, we check than the selections reject a large fraction of data events in those regions while retaining a large fraction of the MC. The following variables are selected:

- **High and low region in the hadronic tag side**:
  - nGoodTracks-pi-int<3
  - nTracks-pi-posThrust<2
- **High and low region in the leptonic tag side**:
  - nGoodTracks-pi-int<2
  - nTracks-pi-posThrust<1

  Also, in addition to those selections we applied other common selections, as following:
  - thrustAxisCosTheta>0
  - vertex-sig-chiProb>0
  - tau-signal-chiProb >0
  - nPhotons-signal <1

8.2 Muon Channel

For the decay mode $\tau^{\pm} \rightarrow \mu^{\pm} K_s^0$, we use the same data luminosity ($189.9 fb^{-1}$), and MC ($6 ab^{-1}$). The following selection criteria, which were optimized on MC, are applied:

- $0.0 < M_{\mu}$ tag photons < 8
- tau tag p CMS < 4.9
- $0.485 < K_s^0$ signal M < 0.51
- M_{π} tag photons < 1.6
- -0.96 $< K_s^0$ signal cosHelicityAngleMomentum < 0.96

Comparing the data/MC in both signal channels, one can notice that in case of the electron channel, the signal is higher than muon channel, that is because we use different samples for MC data events.

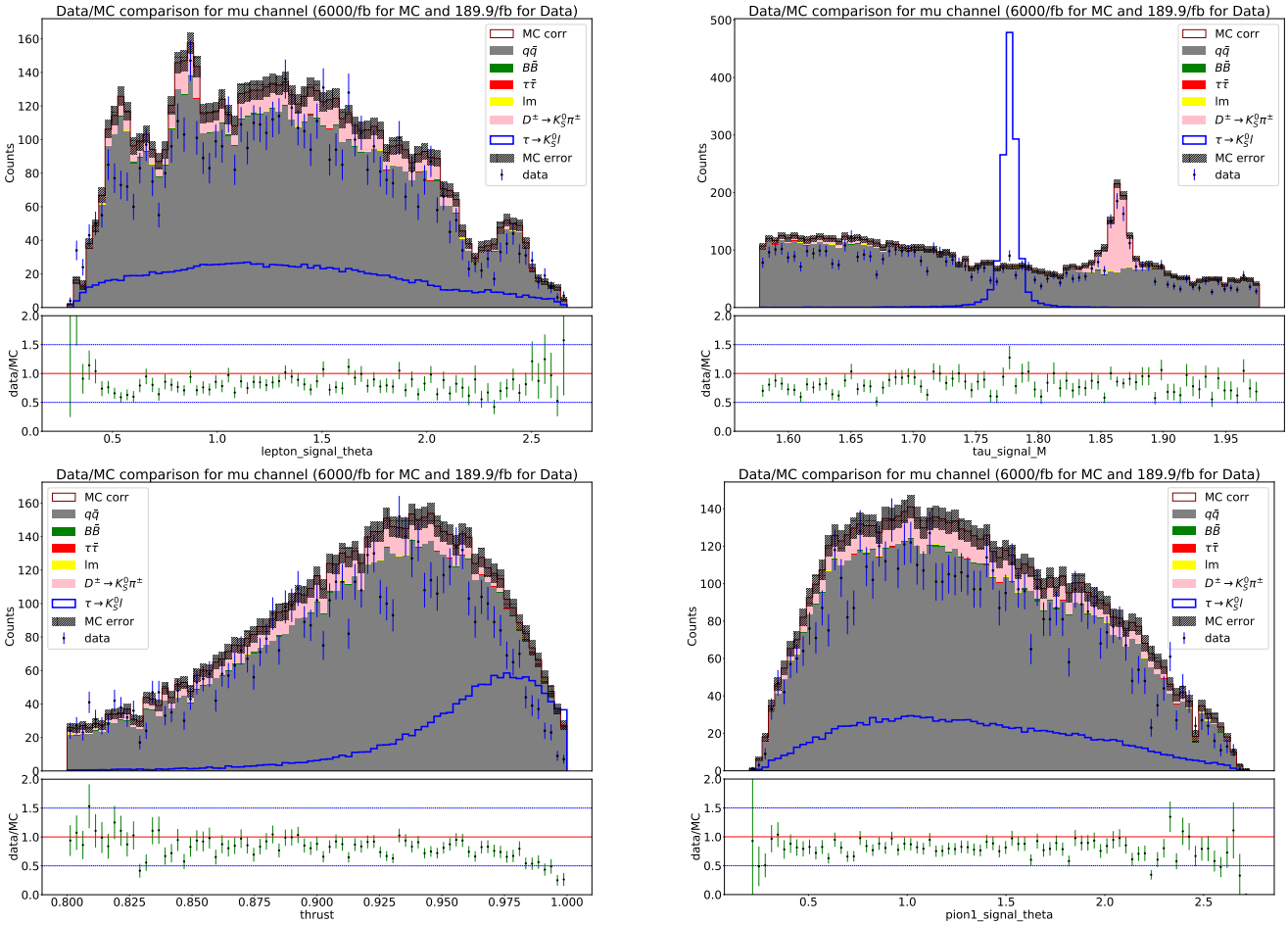

Figure 22: Data/MC comparison after applying moun selections.

9 Conclusion

After applying all the selections criteria above to our data frames, we combine them again with the middle region and check the data/MC comparison. In fig23, it shows a good agreement for our data/MC comparison which becomes better after applying the trigger lines, offline reconstructions, and finally the selection candidates help to reach the goal.

The work done for this report presents data to MC comparison for the $\tau^{\pm} \to l^{\pm} K_s^0$ analysis. In the first part the comparison was performed for the reference channel $D^{\pm} \to K_s^0 \pi^{\pm}$, which has similar decay kinematics and could therefore be used as proxy to validate the data/MC agreement. A second part compares data and MC reconstructed for the signal decay $\tau^{\pm} \to l^{\pm} K_s^0$ in the sideband regions. Results from this study will lead to a systematic uncertainty on the number of expected background events in the signal region. The analysis takes into account some factors to optimize the agreement between the real data and MC. Trigger bits are one of these factors which applied to the real data and MC in line with the trigger efficiency corrections for the data/MC comparison.
Signal candidates are examined in two dimentional plots, the invariant mass and ΔE of the τ, in $3\sigma, 5\sigma, 20\sigma$ regions. The analysis is done outside 5σ region for the electron channel. Several additional selections are added to the data frames to cut on the undesired events and reach to the agreement for data and MC. The situation for the data/MC comparison is good in the electron channel but still need other corrections for the reconstructed K_s^0. Once data and MC show satisfying agreement and systematic errors coming from the comparison are evaluated, the signal region can be opened and the upper limit calculated.

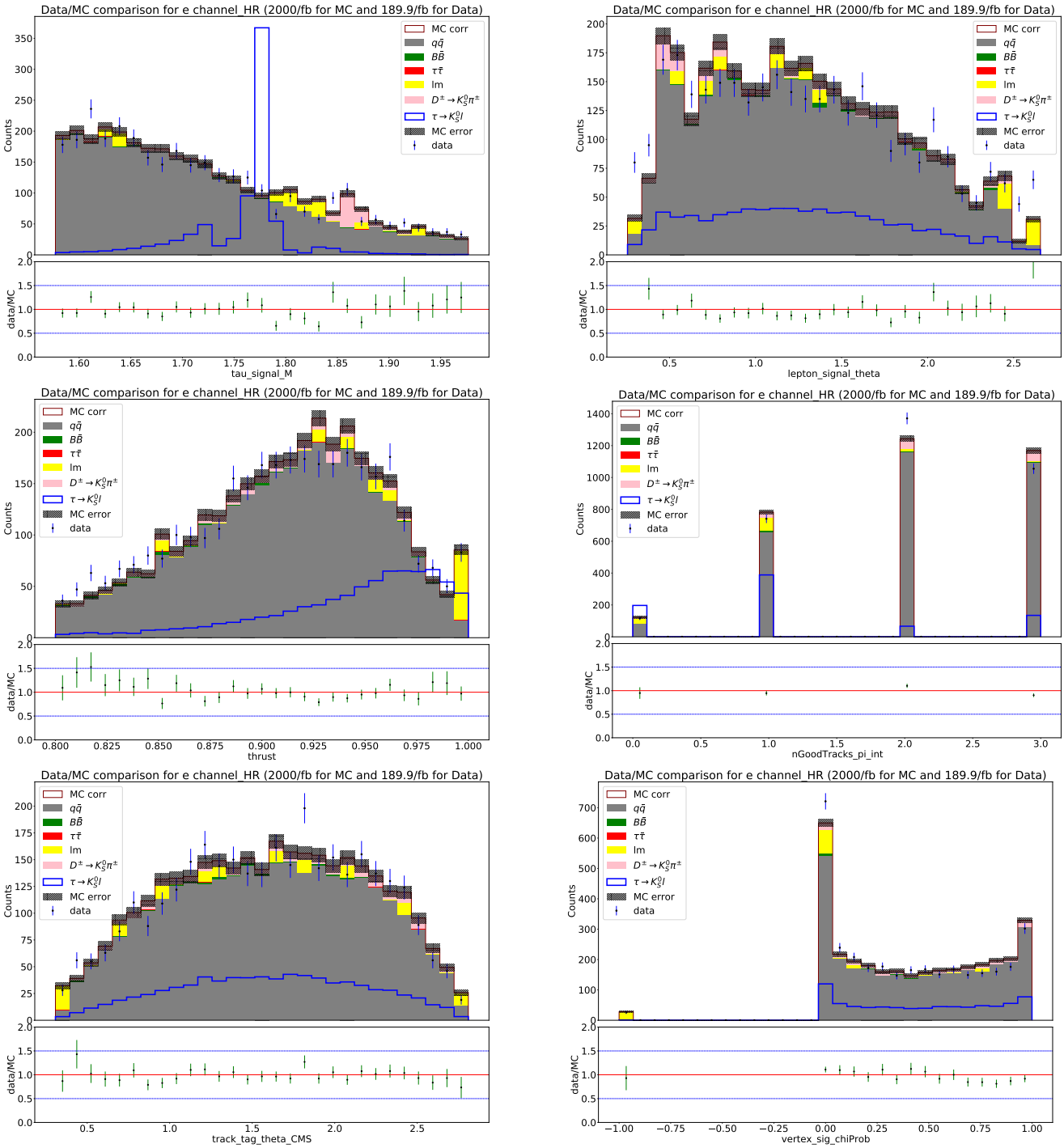

Figure 23: Data/MC comparison after the selections that applied to the high and low region

A Appendix

∗ **Trigger Definitions**:

- **fff** : 3 full tracks.
- **ffo** : >= 2 full tracks, track pair with $\Delta\phi$> 90° and not an ECL Bhabha.
- **ffy** : full tracks>=3, |z|<20cm .
- **ffs** : >=2 full tracks, 1 short tracks.
- **lml0** : >= 3 clusters with at least one having E^*> 300 MeV, 1 < θ_{id} < 17 (corresponding to 18.5°< θ< 139.3°. full ECL) and not an ECL Bhabha.
- **lml1** : 1 cluster with E>2 GeV and 4 <θ_{id} < 14 (32.2° < θ< 124.6°)
- **lml2** : >=1 cluster with E> 2 GeV, θ_{id}= 2, 3, 15, or 16 (18.5° < θ< 32.2° or 124.6°<θ < 139.3°) and not an ECL Bhabha.
- **lml3** : one cluster >= 2 GeV(CM) with θ_{id} = 2, 3, 15 or 16 and an ECL 3D Bhabha.
- **lml4** : >=1 cluster with E^*>2 GeV, θ_{id} =1 or 17 (θ< 18.5° or θ > 139.3°) and not an ECL Bhabha.
- **lml5** : one cluster 2 GeV(CM) with θ_{id} = 1 or 17 and an ECL 3D Bhabha.
- **lml6** : 1 cluster with E^*>1 GeV. 4<θ_{id}<15 (32.2° < θ< 128.7°, full ECL barrel) and no other cluster with E> 300 MeV.
- **lml7** : 1 cluster with E^*>1 GeV. θ_{id} =2, 3 or 16 (18.5°<θ< 31.9° or 128.70° <θ>139.3°) and no other cluster with E >300 MeV.
- **lml8** : cluster pair with 170°<$\Delta\phi$< 190°, both clusters with E> 250 MeV and no 2 GeV cluster in the event.
- **lml9** : cluster pair with 170° <$\Delta\phi$< 190°, one cluster with E^*> 250 MeV with the other having E^*>250 MeV, and no 2 GeV cluster in the event.
- **lml10** : cluster pair with 160° <$\Delta\phi$< 200°. 160°< $\sum\theta$ < 200° and no 2 GeV cluster in the event.
- **lml11** : No 2GeV(CM) cluster in an event
- **lml12** : 3 cluster with at least me having E^*> 500 MeV 2<θ_{id}< 16 (corresponding to 18.5 < Δ< 139.3. full ECL) and not an ECL Bhabha. modified trigger bit of lml0.
- **lml13** : only one cluster >= 0.5 GeV(CM) with θ_{id} = 6-11 and no other cluster >= 300 MeV(Lab) anywhere. modified trigger bit of lml6.

Variables for studying the comparison after applying trigger efficiency corrections, figA

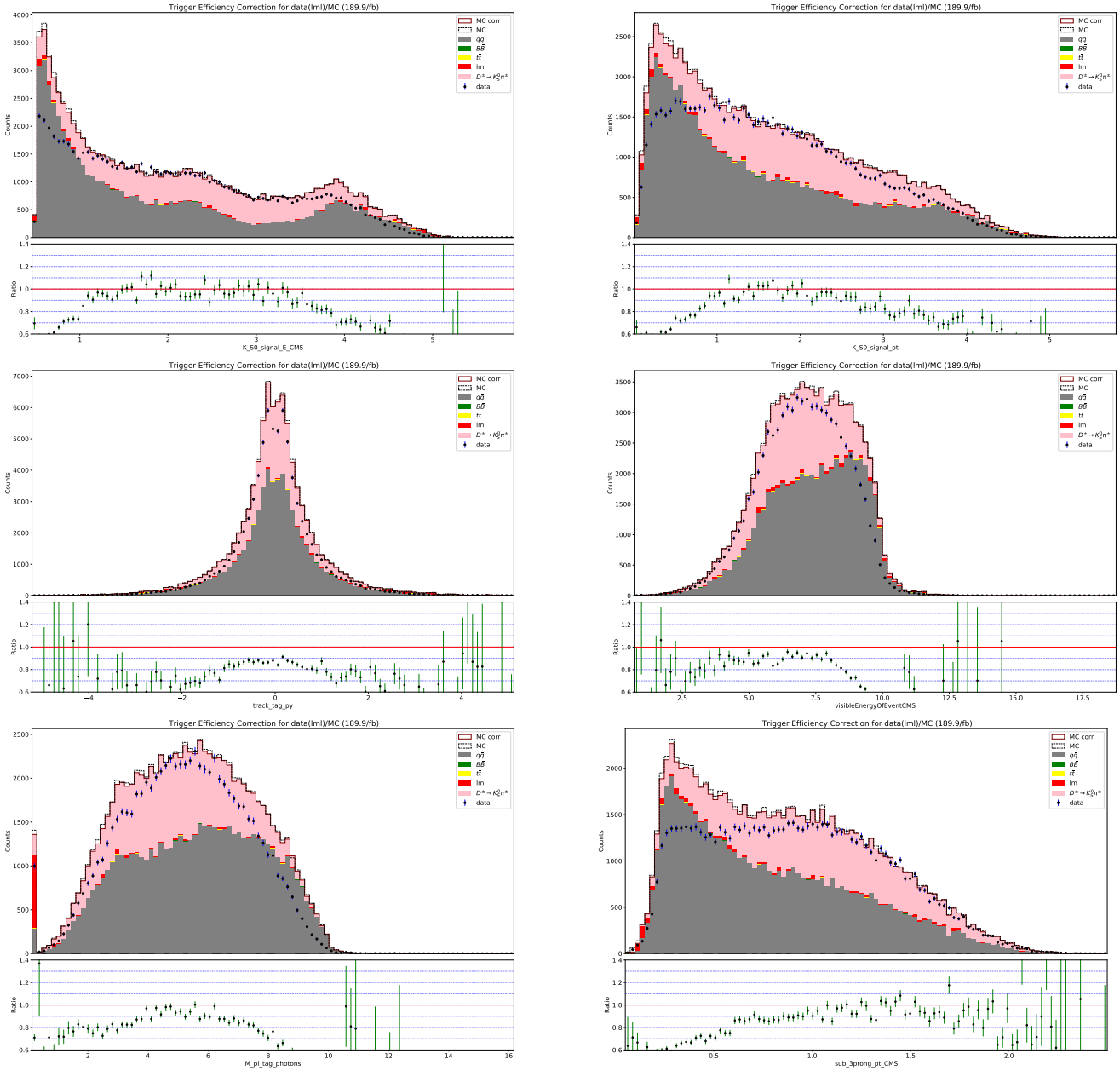

Figure 24: Data/MC after applying corrections of trigger selections

Variables for studying the comparison after applying muon selections, figA

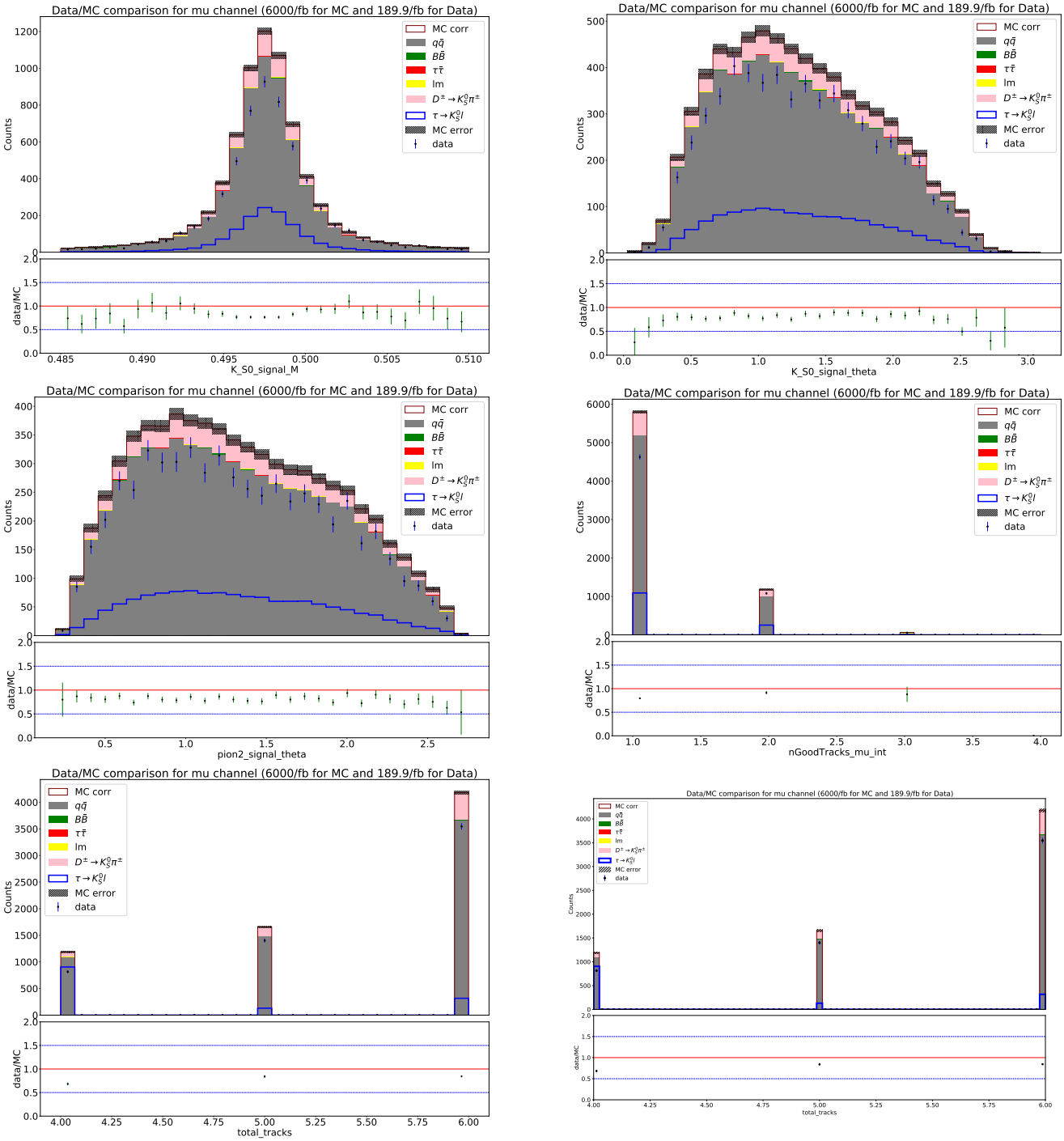

Figure 25: Data/MC after applying muon selections

Variables for studying the comparison after applying electron selections, figA

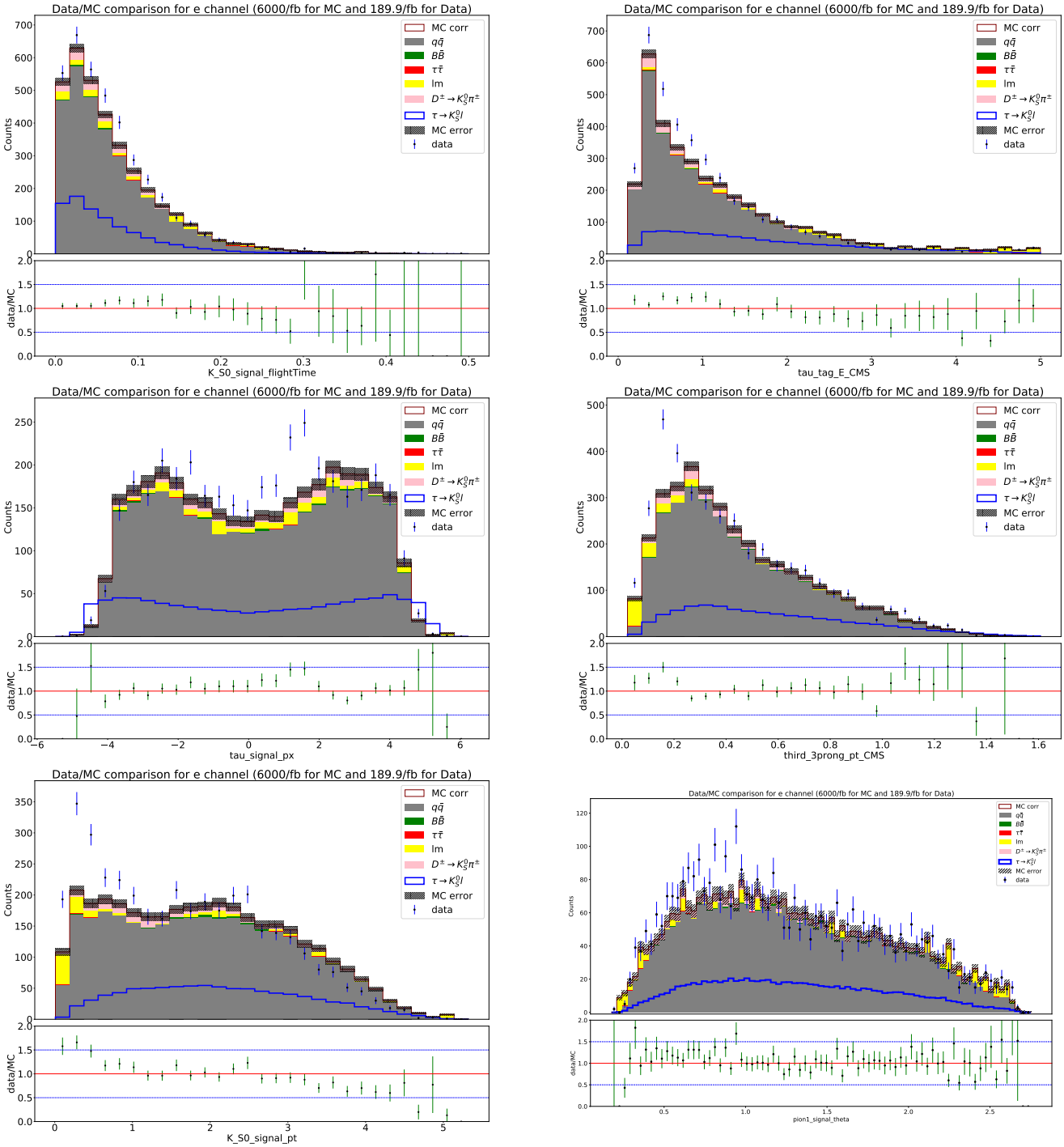

Figure 26: Data/MC after applying electron selections

Other variables for data/MC comparison after applying the selections that applied to the high and low region figA

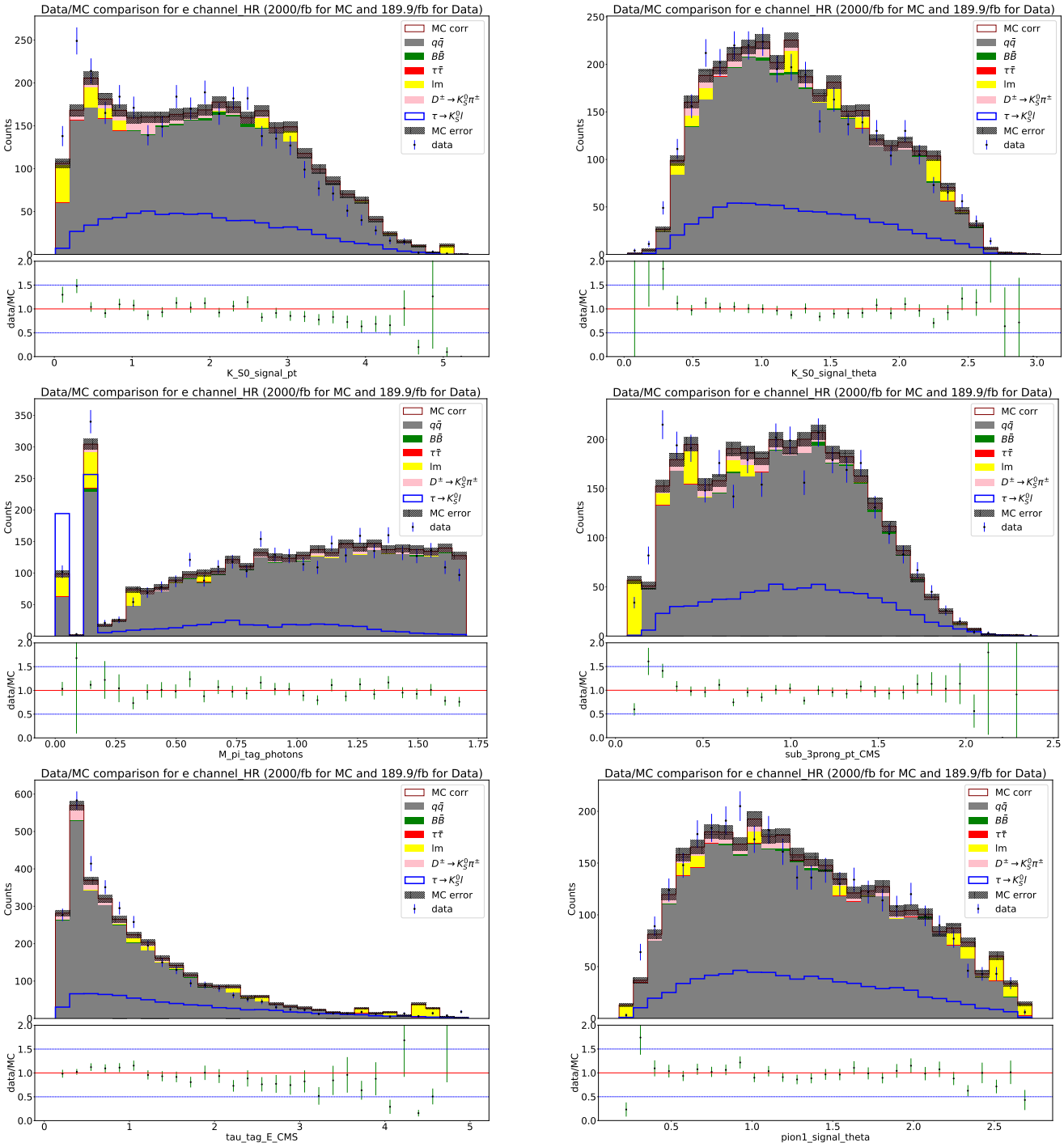

Figure 27: Data/MC comparison after the selections that applied to the high and low region

B References

References

[1] The Belle II Physics Book

[2] Search for Lepton Flavor Violating τ Decays into $l^- K_s^0$ and $l^- K_s^0 K_s^0$. DOI: https://doi.org/10.1016/j.physletb.2010.07.012.

[3] Y.Ohnishi et al. "Accelerator design at SuperKEKB". In: Progress of Theoretical and Experimental Physics 2013.3 (Mar. 2013). DOI: 10.1093/ptep/pts083.

[4] M. Tanabashi et al. "Review of Particle Physics". In: Phys. Rev. D 98 (3 Aug. 2018), p. 030001. DOI: 10.1103/PhysRevD.98.030001.

[5] Beyond the Standard Model: supersymmetry. I. Antoniadis1 and P. Tziveloglou2. CERN, Geneva, Switzerland.

[6] Revised August 2021 by S. Rolli (DOE) and M. Tanabashi (Nagoya U.; KMI, Table 94.1: Possible leptoquarks and their quantum numbers.

[7] Searches for lepton flavor violation in tau decays are unambiguous signatures of new physics. The branching ratios of tau leptons. https://arxiv.org/pdf/2209.11639.pdf.

[8] Comprehensive study of the background for the Pixel Vertex Detector at Belle II Andreas Moll. DOI: 10.5282/edoc.19106.

[9] Lepton Flavour Violation Theory, Thorsten Feldmann: https://arxiv.org/abs/1105.2139

[10] The model-discriminating power of lepton flavor violating decays Alejandro Celis, Vincenzo Cirigliano and Emilie Passemar: https://arxiv.org/pdf/1403.5781.pdf